Physisorbed films in periodic mesoporous silica studied by *in situ* synchrotron small-angle diffraction

Gerald A. Zickler,[1] Susanne Jähnert,[2] Wolfgang Wagermaier,[1] Sérgio S. Funari,[3] Gerhard H. Findenegg,[2] and Oskar Paris[1,*]
[1]*Department of Biomaterials, Max Planck Institute of Colloids and Interfaces, D-14424 Potsdam, Germany*
[2]*Stranski Laboratory of Physical and Theoretical Chemistry, Technical University Berlin, Straße des 17. Juni 135, D-10623 Berlin, Germany*
[3]*Hamburger Synchrotronstrahlungslabor (HASYLAB), Deutsches Elektronen-Synchrotron (DESY), Notkestraße 85, D-22603 Hamburg, Germany*
(Received 23 December 2005; revised manuscript received 6 March 2006; published 8 May 2006)

Adsorption and capillary condensation of an organic fluid in a periodic mesoporous silica (SBA-15) are studied by *in situ* synchrotron diffraction. Powder diffraction patterns resulting from the two-dimensional hexagonal packing of the cylindrical pores of SBA-15 are collected as a function of vapor pressure during continuous adsorption and desorption of the fluid (perfluoropentane C_5F_{12}), using a specially designed sorption cell. Seven diffraction peaks with systematic changes of the intensity are resolved as the adsorbed film thickness increases along the adsorption isotherm. The integrated intensities of the diffraction peaks are analyzed with a structural model involving four levels of electron density (dense silica matrix, microporous corona around the pores, adsorbed film, and core space of the pores). The model provides quantitative information about the structure of the evacuated specimen, the filling of the corona, and the growing thickness of the liquid film with increasing pressure. A very good fit of the data by this model is found for relative pressures up to $p/p_0 \approx 0.5$, but the fit of the high-indexed diffraction peaks becomes poor close to the capillary condensation pressure ($p/p_0 \approx 0.68$). Tentatively, this fact may be attributed to a deviation of the liquid film structure from the simple flat geometry close to the phase transformation, presumably caused by density fluctuations.

DOI: 10.1103/PhysRevB.73.184109 PACS number(s): 81.07.−b, 64.70.Fx, 61.10.Eq, 07.85.Qe

I. INTRODUCTION

Mesoporous materials are of importance for a wide range of technical applications such as gas storage, separation processes, and heterogeneous catalysis, and much progress has been made in the design, synthesis, and characterization of materials with novel properties.[1,2] It is well known that the filling of nanometer-sized pores proceeds via the formation of an adsorbed film, which is growing in thickness with increasing vapor pressure, until a sharp increase of the adsorbed amount occurs due to capillary condensation of the vapor.[3] Capillary condensation represents a first-order phase transition in a confined geometry and commonly exhibits a pronounced hysteresis with respect to adsorption and desorption. The physics of capillary condensation is attracting much attention because it is of great practical relevance, as it forms the basis of the pore-size determination by gas adsorption.[4] The pore size can be determined from the pore condensation pressure of the gas on the basis of either the Kelvin equation or the density functional theory,[5] but both methods rely on a knowledge of the thickness of the adsorbed film at the pore wall.[6] For open, flat surfaces, the thickness of adsorbed films can be determined directly by ellipsometry,[7] x-ray reflectometry,[8] or the quartz-crystal balance,[9] but none of these techniques is able to measure the film thickness in narrow pores.

Small-angle scattering techniques are widely used for the determination of the specific surface area, pore size, and wall architecture of mesoporous and microporous materials. For the *in situ* investigation of liquid sorption effects by scattering of x rays[10–13] or neutrons,[14–16] special adsorption cells were developed. An overview is given by the review article of Hoinkis.[17] However, only few attempts were made in these studies to interpret the scattering data quantitatively in terms of the different sorption processes. Smarsly *et al.*[16,18] investigated nitrogen sorption in porous silica by *in situ* small-angle neutron scattering. The data were analyzed by using chord-length distribution and analytical model functions and the results were compared with high-resolution adsorption porosimetry.

For materials with a periodic pore structure, structural information can be obtained from diffraction data by analyzing the intensity of the individual diffraction peaks arising from the periodic arrangement of the pores.[19] Recently, this method was adopted to determine the thickness of physisorbed films in pores using small-angle x-ray diffraction[12,13] or small-angle neutron diffraction.[20] The present work pursues this approach and shows that detailed information about the adsorbed film of an organic vapor in the pores of SBA-15 silica can be obtained by *in situ* synchrotron small-angle diffraction.

SBA-15 like the better-known MCM-41 silica constitutes a two-dimensional hexagonal array of cylindrical pores of uniform size. In view of their well-defined mesopore structure, these materials have been used for model studies of capillary condensation[21–25] and mesopore size determination.[26–30] For a periodic array of ideal cylindrical pores with smooth walls embedded in a matrix of uniform density, the pore radius can be evaluated from the pore-to-pore center distance, the specific pore volume, and the density of the matrix.[29,31] For a given pore radius R, the thickness of the adsorbed film t can be estimated from the degree

of pore filling f by the relation $t=R[1-(1-f)^{1/2}]$. However, several recent studies have indicated that SBA-15 silica does not represent such an ideal matrix,[2,19,31] as the cylindrical mesopores appear to be surrounded by a corona which may either represent a microporous layer[19] or result from pronounced surface corrugations of the pore walls.[32] The influence of this microporous corona on the pore filling of SBA-15 silica was investigated in two recent small-angle diffraction studies: The adsorption and pore condensation of krypton in SBA-15 were studied by Hofmann *et al.*[12] using x-ray diffraction, and a similar study for nitrogen in SBA-15 was performed by Schreiber *et al.*[20] using small-angle neutron diffraction. In these studies, structural information about the adsorbed film is derived from the intensities of the diffraction peaks, which result from the regular packing of the pores. The accuracy of film thickness determination depends on the number of diffraction peaks that can be resolved independently. In this respect, x rays are superior to neutrons due to smaller wavelength dispersion, allowing a better resolution of the individual diffraction peaks without overlap. Hofmann *et al.*[12] used a rotating-anode x-ray source and up to five diffraction peaks were resolved, though the higher-order peaks suffered from insufficient statistical accuracy. Therefore, the choice of the model for the adsorbed film was dictated by the necessity to minimize the number of independent fit parameters.

In order to extract more specific information about the adsorbed film in the pores it is desirable to increase the number of resolvable diffraction peaks. In the present work synchrotron x-ray diffraction is used to study *in situ* the pore filling of SBA-15 silica with an organic fluid. A dedicated setup with high resolution and low background allows detection of seven clearly separated peaks with high statistical accuracy. A structural model, going beyond the one used in the recent work by Hofmann *et al.*,[12] is developed to analyze the evolution of the adsorbed film as a function of pore filling. We compare the results of the present work with results from literature and with predictions from theory, and we discuss the limitations of simple flat-film models for pressures close to capillary condensation.

II. EXPERIMENTAL METHODS

A. Sample preparation and characterization

SBA-15 silica was synthesized according to the prescription of Zhao *et al.*,[33,34] using a technical triblock copolymer (Pluronic-123, BASF) as the structure-directing template in aqueous H_2SO_4 solution, and tetraethyl orthosilicate as the silicate source. The synthesis, hydrothermal treatment, and calcination of the product followed a similar protocol as given by Hofmann *et al.*[12]

The sample was characterized by nitrogen adsorption at 77 K. Its Brunauer-Emmett-Teller[3,6] specific surface area a_s was 785 $m^2\ g^{-1}$ (based on the adsorption data in the pressure range $0.05<p/p_0<0.30$ and an area per nitrogen molecule of 0.162 nm^2) and the total specific pore volume v_p was

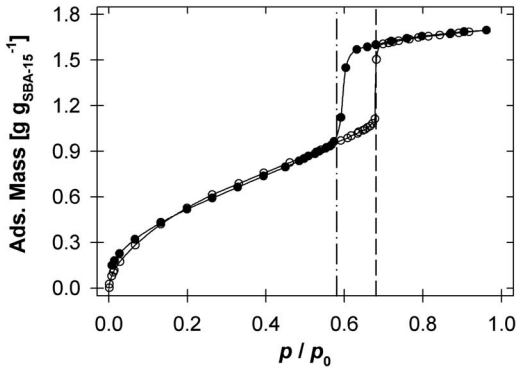

FIG. 1. Adsorption isotherm (open symbols) and desorption isotherm (filled symbols) of C_5F_{12} in SBA-15 at 20 °C expressed as adsorbed mass versus relative pressure p/p_0. The two vertical lines indicate the relative pressures of capillary condensation (dashed) and capillary evaporation (dash-dotted).

1.033 $cm^3\ g^{-1}$ (based on the adsorbed amount at relative pressure $p/p_0=0.98$ and the density of liquid nitrogen at 77 K, $\rho=0.8086$ g cm^{-3}). The radius of the cylindrical pores was determined from the desorption branch of the hysteresis loop by the nonlocal density functional theory (NLDFT) kernel,[29] which gives a value $R_{DFT}=4.1$ nm, in agreement with the value R_{BJH} obtained by the classical Barrett-Joyner-Halenda (BJH) pore-size analysis from the adsorption branch of the hysteresis loop with the de Boer standard isotherm.[6]

Perfluoropentane (C_5F_{12}, ABCR Chemicals, purity >97%, 85% *n* isomers) was used as received. The adsorption isotherm of C_5F_{12} in the present sample of SBA-15 was determined over a pressure range from 10^{-4} bar to the saturation pressure p_0 ($p_0=0.706$ bar at 20 °C) using a vacuum microbalance method described elsewhere.[35] The sorption isotherm for 20 °C is shown in Fig. 1. It exhibited three typical regions, corresponding to monolayer and multilayer adsorption, capillary condensation, and further adsorption onto the external surface of the SBA-15 grains. The shape of the isotherm was characteristic of mesoporous materials (type IV isotherm according to IUPAC classifications),[3] exhibiting a marked hysteresis loop with a shape corresponding to capillary condensation in open cylindrical pores. The adsorption and desorption branches of the hysteresis loop were very steep, as to be expected for a narrow pore-size distribution.

B. Synchrotron x-ray diffraction experiments

For *in situ* small-angle synchrotron x-ray diffraction in conjunction with sorption, a special cell was designed. The specimen chamber was made of aluminum and the cell windows were equipped with Kapton foils. SBA-15 powder was pressed to a stable pellet of 0.3 mm thickness and 3 mm diameter. The adsorption cell was temperature controlled by Peltier devices and had an internal flow system, which was connected via pipes to the liquid adsorbent (C_5F_{12}) in a reservoir. The gas was conducted through a needle valve to the sample in the sorption chamber, where the vapor pressure was measured with a Baratron capacitance manometer (MKS

Instruments). Before starting an experiment, the specimen was evacuated at a temperature of 80 °C and a pressure below 10^{-5} mbar for 1 h. For sorption experiments, the cell was cooled to 17 °C to be the coldest point in the system and the reservoir stayed at ambient temperature of 21 °C. The whole setup was remote controlled by a custom-written software program based on HP VEE,[36] which allowed continuous adsorption and desorption scans.

Small-angle x-ray diffraction measurements were performed at the beamline A2 (Ref. 37) at Hamburger Synchrotronstrahlungslabor (HASYLAB)/Deutsches Elektronen-Synchrotron (DESY) in Hamburg, Germany. Synchrotron radiation was monochromatized by a germanium (111) crystal to an energy E of 8.27 keV ($\Delta E/E=10^{-3}$), focused by a single mirror, and the beam cross section was defined by aperture slits to 2 mm (horizontally) $\times$ 0.5 mm (vertically) at the sample position. A charge-coupled device x-ray area detector (MarCCD 165, Marresearch) with a resolution of 2048×2048 pixels (pixel size 79×79 μm^2) was used to detect the scattered photons. The precise sample-to-detector distance of 1425.6 mm was determined by calibration with silver behenate. The x-ray diffraction patterns covered a range of the scattering vector q of $0.3<q<2.4$ nm^{-1}. The length of the scattering vector is given by $q=4\pi/\lambda \sin\theta$, with 2θ being the scattering angle and λ the wavelength. Vacuum flight tubes were inserted between sample and detector in order to avoid air scattering. The transmission of all samples at each sorption state was determined *in situ* by using an ionization chamber before the adsorption cell to monitor the primary synchrotron x-ray flux and a photodiode mounted in the beamstop to measure the transmitted photons. A typical exposure time of 60 s yielded a scattering pattern with excellent measuring statistics. The scattering patterns were corrected for background scattering, electronic noise, transmission, and polarization by using the data reduction program FIT2D.[38] All specimens showed isotropic scattering patterns, which were azimuthally averaged for equal radial distances from the central beam.

III. RESULTS AND DATA ANALYSIS

A. X-ray diffraction profiles and integrated peak intensities

Figure 2 shows a series of small-angle x-ray diffraction profiles of SBA-15 at various relative pressures of C_5F_{12}. Five diffraction peaks [corresponding to the (10), (11), (20), (21), and (30) diffractions of the two-dimensional hexagonal lattice] are visible for the evacuated sample. The diffraction peaks change their intensities with increasing vapor pressure and two additional peaks (22) and (31) become clearly visible with continuous adsorption.

After exceeding the pore condensation point, a strong decrease of peak intensities is observed. These effects are fully reversible, i.e., after desorption the initial state is reached again. In addition to the diffraction peaks, a diffuse small-angle scattering signal is observed, which also changes with varying vapor pressure. This signal may be correlated to other weakly ordered heterogeneities, which are also affected (e.g., filled) during adsorption.

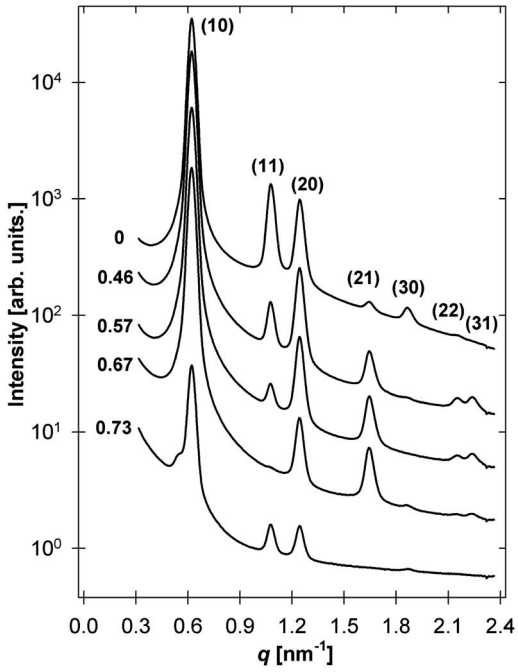

FIG. 2. A typical series of small-angle x-ray diffraction profiles (scattering intensity versus length of scattering vector) during adsorption of C_5F_{12} in SBA-15. For the sake of clarity, the curves are shifted vertically by a factor of 3 with respect to each other. The values given at the left side of the figure refer to relative pressures p/p_0. The top four profiles were measured at pressures below the pore condensation point and the last profile was measured above the pore condensation point.

For the following analysis, the diffuse scattering is treated as a continuous background and the integrated intensity $\tilde{I}(q_{hk})=\int I(q_{hk})q^2dq$ of each diffraction peak is calculated. A custom-written program based on the free software PYTHON (Ref. 39) and GNUPLOT (Ref. 40) is used to fit each peak separately with a pseudo-Voigt function and a linear background. The position, width, and height of the peaks are free fit parameters and no constraints are set. Figure 3 shows the integrated intensities as a function of relative pressure during adsorption and desorption of C_5F_{12} in SBA-15 for all measured diffraction peaks. The curves show characteristic changes of the integrated intensity and for all peaks a distinctive hysteresis is observed in the region of capillary condensation. Besides the integrated intensities, the positions of the peaks are used to calculate the lattice parameter a of the pore lattice (Table I).

B. Structure model for sorption

For data interpretation, a structure model for *in situ* adsorption and desorption is developed, following closely the studies of Impéror-Clerc *et al.*,[19] where a model involving a corona of uniform density was used. It is assumed that the cylindrical mesopores are perfectly ordered in a two-dimensional hexagonal lattice and that the mesopores are monodisperse with perfectly circular cross section, but surrounded by a corona of reduced (but uniform) silica density

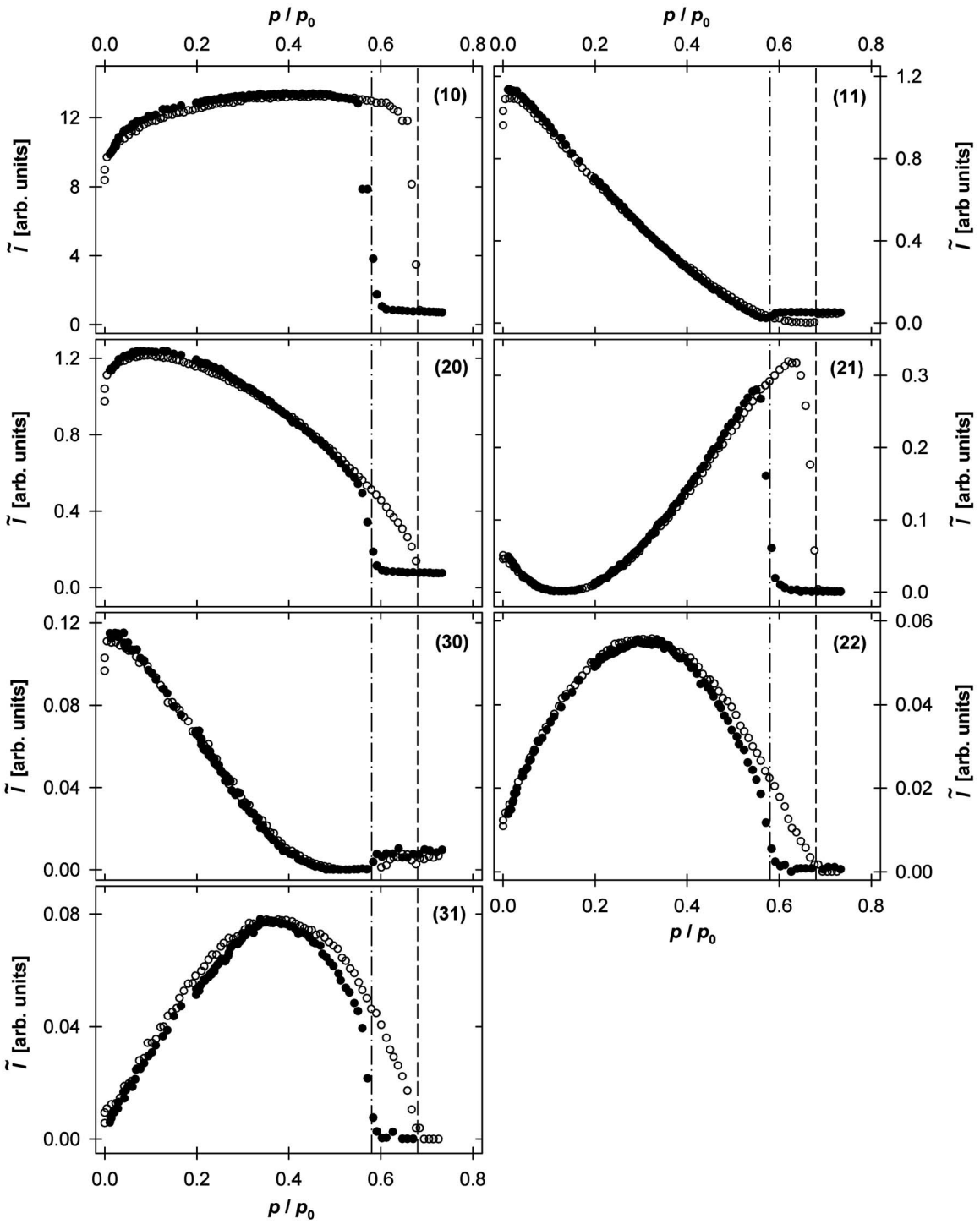

FIG. 3. Integrated intensities $\tilde{I}$ of the first seven x-ray diffraction peaks (10), (11), (20), (21), (30), (22), and (31) for adsorption and desorption scans of C_5F_{12} in SBA-15. The open symbols denote the adsorption scan and the filled symbols indicate the desorption scan. The two vertical lines represent the relative pressures p/p_0 of capillary condensation (dashed) and capillary evaporation (dash-dotted). For comparison see Fig. 1.

due to microporosity, while the outer region consists of dense silica (Fig. 4). The system is isotropic due to the powder form of the material with a grain size of about 200–500 nm. The spherical average of the total scattered intensity $I(q)$ for an assembly of very long cylindrical objects is given by

$$I(q) = KS(q)|F(q)|^2, \tag{1}$$

with the structure factor $S(q)$ and the form factor $|F(q)|^2$, $F(q)$ being the scattering amplitude of the cylindrical cross section, and K a constant prefactor. A Debye-Waller factor is

TABLE I. Lattice parameter a, radii R_1 and R_2, and porosity of the corona P of the present SBA-15 sample and values of the study of Impéror-Clerc *et al.* (Ref. 19). The value of R_2 is compared with the pore size determined from the nitrogen sorption isotherm on the basis of the density functional theory (DFT) and the Barrett-Joyner-Halenda (BJH) model, respectively.

	X-ray diffraction		N_2 sorption	
Parameter	Present sample	P 123 BC[a]	DFT	BJH
a (nm)	11.64±0.05	11		
R_1 (nm)	5.15±0.15	4.7		
R_2 (nm)	3.95±0.05	3.5	4.1	4.1
P	0.41±0.05	0.55		

[a]Reference 19.

not introduced, since it turns out that our data can be well described with Eq. (1) without taking thermal or static lattice distortions into account. For a perfect two-dimensional hexagonal lattice, the spherically averaged structure factor $S(q)$ is given by

$$S(q) = \frac{1}{q^2}\sum_{hk} M_{hk} S_{hk}(q). \tag{2}$$

M_{hk} is the multiplicity factor of the diffraction peaks [$M_{hk}=12$ for diffractions of mixed Miller indices (hk), and $M_{hk}=6$ for $(h0)$ and (hh)] and S_{hk} are δ functions at positions

$$q_{hk} = \frac{4\pi}{a\sqrt{3}}\sqrt{h^2+k^2+hk}, \tag{3}$$

where a is the lattice parameter. The scattering amplitude $F(q)$ for a number N of nested cylindrical shells can be written in analogy to spherical shells[41]

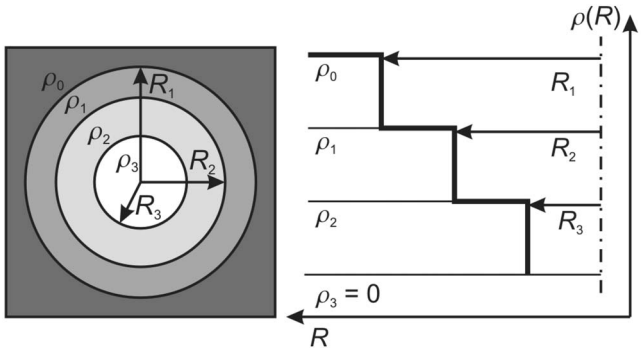

FIG. 4. Model of the pore structure of SBA-15 with four density levels, viz., dense silica matrix (electron density ρ_0), microporous corona (electron density ρ_1), adsorbed liquid film (electron density ρ_2), and vapor in the core of the pore (electron density $\rho_3=0$). R_1, R_2, and R_3 represent the corresponding radii of the different shells. $R_3=0$ at relative pressures p/p_0 above the phase transition.

$$F(q) = \frac{\sum_{i=1}^{N}(\rho_i-\rho_{i-1})R_i^2 Z(qR_i)}{\sum_{i=1}^{N}(\rho_i-\rho_{i-1})R_i^2}, \tag{4}$$

where ρ_i is the electron density and R_i the radius of the ith shell, starting from the outermost shell. The function Z is given by $Z(qR)=2J_1(qR)/(qR)$, J_1 being the Bessel function of the first kind of first order.[42] For the special case of sorption in SBA-15, the four-density-level model depicted in Fig. 4 is chosen, where the scattering amplitude is explicitly given by

$$F(q) = \frac{(\rho_1-\rho_0)R_1^2 Z(qR_1) + (\rho_2-\rho_1)R_2^2 Z(qR_2) + (\rho_3-\rho_2)R_3^2 Z(qR_3)}{(\rho_1-\rho_0)R_1^2 + (\rho_2-\rho_1)R_2^2 + (\rho_3-\rho_2)R_3^2}. \tag{5}$$

Equation (5) can be used to fit the measured integrated intensities $\tilde{I}(q_{hk})$ by minimizing the variance

$$\chi^2 = \sum_{hk}\left|\left(\left[\frac{\tilde{I}(q_{hk})}{M_{hk}}\right] - [K|F(q)|^2]\right)\right|^2. \tag{6}$$

Only the parameters R_3 (defined by the film thickness of the growing liquid layer) and ρ_1 (electron density of the corona) in Eq. (5) are expected to depend on the gas pressure p/p_0 during a sorption experiment. All other parameters (R_1, R_2, ρ_0, ρ_2, and ρ_3) are constant. Generally, pore filling by the fluid involves the following stages, which help to reduce the number of independent fit parameters for each stage. The following notations are used: $\alpha=\rho_1/\rho_0$ and $\beta=\rho_2/\rho_0$, with the electron densities of bulk silica $\rho_0=\rho_{\text{Silica}}=6.52\times10^{23}$ cm^{-3} and bulk adsorbing liquid (C_5F_{12}) $\rho_2=\rho_{\text{liquid}}=4.67\times10^{23}$ cm^{-3}.

1. Evacuated sample and regime of corona filling

With $\rho_3=0$ for the evacuated pores and $R_3=R_2$ before the onset of film growth, Eq. (5) reduces to $F(q)=F_1(q)$, with

$$F_1(q) = \frac{(\alpha-1)R_1^2 Z(qR_1) - \alpha R_2^2 Z(qR_2)}{(\alpha-1)R_1^2 - \alpha R_2^2}. \tag{7}$$

For the completely evacuated specimen, Eq. (7) is used to determine the radii R_1 and R_2, to define the corona and pore radius, as well as the microporosity of the corona $P=1-\alpha_{\text{evac}}$ [with $\alpha_{\text{evac}}=\alpha(p/p_0=0)$]. The resulting values of R_1 and R_2 are determined and kept constant during fitting of the

subsequent stages of pore filling. The results indicate that in a region at low gas pressure the parameter α increases while all other parameters remain constant, as is to be expected for the filling of a microporous corona. After complete filling of the pores, $\alpha_{\text{full}}=P\beta+(1-P)$ is determined by the known values of P (from the evacuated material) and β (from the known electron densities of silica and the adsorbing liquid). However, α may not reach this limiting value due to incomplete filling of the corona (e.g., closed pores or exclusion of filling due to molecule size). Moreover, corona filling and continuous film growth may be two concomitant processes at higher gas pressures.

2. Simultaneous corona filling and film growth

For the regime of simultaneous corona filling and liquid film growth, $\rho_3=0$ and $R_3<R_2$, and Eq. (5) becomes $F(q)=F_2(q)$ with

$$F_2(q)=\frac{(\alpha-1)R_1^2Z(qR_1)+(\beta-\alpha)R_2^2Z(qR_2)-\beta R_3^2Z(qR_3)}{(\alpha-1)R_1^2+(\beta-\alpha)R_2^2-\beta R_3^2}. \tag{8}$$

Equation (8) is used with fixed values of β, R_1, and R_2. The only fit parameters in this regime are α and R_3, and as a further constraint it is assumed that α should increase or remain constant, while R_3 must either remain constant or decrease with increasing pressure. It can be expected that α increases until it reaches the limiting value α_{full}, while R_3 is constant at the beginning ($R_3=R_2$) and is expected to decrease then continuously until pore condensation.

3. Filled mesopores

In the case of completely filled mesopores, $R_3=0$, $\rho_3=0$, and $F(q)=F_3(q)$, with

$$F_3(q)=\frac{(\alpha-1)R_1^2Z(qR_1)+(\beta-\alpha)R_2^2Z(qR_2)}{(\alpha-1)R_1^2+(\beta-\alpha)R_2^2}, \tag{9}$$

which has the same form as Eq. (7) except for the contrast.

4. Mesopore condensation

A special case is the region of mesopore condensation. Here, the mean density of the pore increases due to liquid bridges of increasing length, and the system can be seen as a two-phase mixture of entirely filled mesopores and mesopores with a liquid film of constant thickness. Neglecting influences of the menisci by assuming that the lengths of filled and unfilled regions are much larger than the pore diameter, and calling γ the fraction of filled mesopores, the behavior of the scattering amplitude during capillary condensation is then given by

$$F(q)=(1-\gamma)F_2(q)+\gamma F_3(q), \tag{10}$$

where $F_2(q)$ and $F_3(q)$ are given by Eqs. (8) and (9), respectively. $\gamma(p/p_0)$ is the only fit parameter and should change from zero to one with increasing pressure in the narrow interval of mesopore condensation. All other parameters, in particular, the thickness of the liquid film determined at the onset of capillary condensation (given by $R_3^{\min}$) are expected to remain constant.

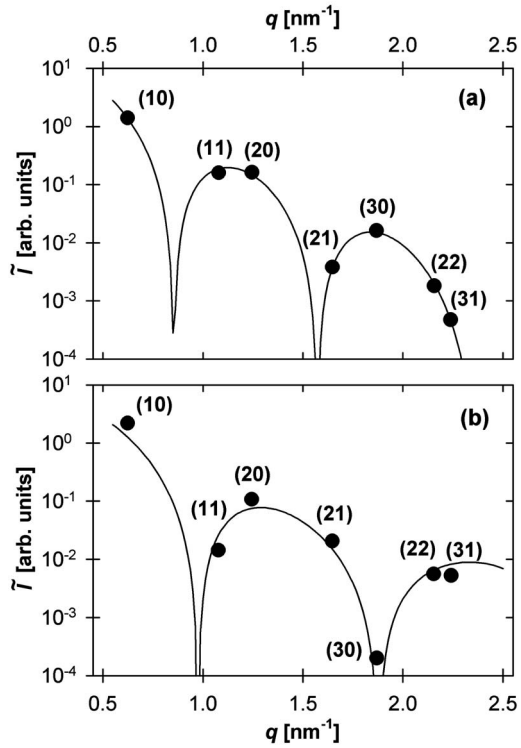

FIG. 5. Examples of experimental integrated intensities $\tilde{I}$ and the corresponding model fits at different relative pressures of C_5F_{12}: p/p_0=(a) 0 and (b) 0.52. The lines denote the model functions according to Eqs. (7) and (8), respectively; the data points are the integrated intensities of the first seven x-ray diffraction peaks of SBA-15.

C. Results from model fitting

Fits are performed with the computer software program MATHEMATICA (Ref. 43) using the NMINIMIZE function and constraints are chosen according to the physical restrictions discussed above. Since the intensity values cover a range of almost four orders of magnitude, logarithmic intensity values are used for fitting. Figure 5 shows examples of experimental integrated intensities and the respective model fits of the evacuated specimen [Fig. 5(a)] and one selected vapor pressure p/p_0 [Fig. 5(b)].

The data from the fully evacuated sample are fitted satisfactorily by using Eq. (7) for the scattering intensity [Fig. 5(a)]. Table I presents the parameters for the evacuated sample. The analysis shows that the three parameters in Eq. (7) are strongly coupled and the minimum of χ^2 [Eq. (6)] is rather flat in the region $0.5<\alpha<0.7$. By taking a 10% increase of χ^2 as a realistic measure of the uncertainty, one gets the error estimates given in Table I.

For the *in situ* gas adsorption and desorption sequences at relative pressures $p/p_0<0.5$, data fitting is performed with Eq. (8) with fixed values of R_1 and R_2 as derived for the evacuated sample. The parameter β is calculated from the known electron densities of bulk silica and bulk liquid C_5F_{12}

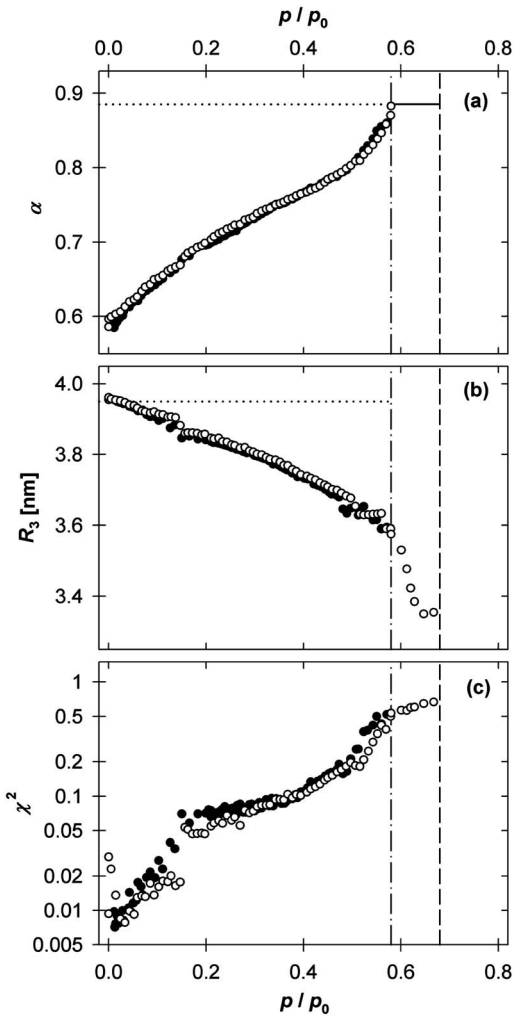

FIG. 6. Fit parameters α and R_3 and the fit variance χ^2 as a function of relative pressure p/p_0 of C_5F_{12} according to the model described in the text. The two vertical lines indicate the relative pressures of capillary condensation (dashed) and capillary evaporation (dash-dotted). For comparison see Fig. 1. The horizontal dotted lines designate the limiting values, determined by parameter studies for evacuated and completely filled material (Table I). Omitted data points indicate that the corresponding parameter is kept constant at the limiting value.

(β=0.717) and is also kept constant. The results are shown in Fig. 6. At low gas pressures, α increases while R_3 starts to decrease from its initial value $R_3=R_2=3.95$ nm at somewhat higher pressures ($p/p_0\approx 0.05$). At $p/p_0\approx 0.58$, α approaches a saturation value $\alpha_{\text{full}}=P\beta+(1-P)=0.88$. Upon capillary condensation, the integrated peak intensities drop drastically and only the first three peaks differ noticeably from zero (Fig. 3). Therefore, no reliable values of the fit parameters can be obtained for pressures $p/p_0>0.68$ along the adsorption isotherm, and for $p/p_0>0.58$ along the desorption isotherm. Figure 6(b) shows that in a wide pressure range, R_3 decreases almost linearly with increasing pressure and reaches a value of about 3.3 nm at the pore condensation pressure, corresponding to a liquid film thickness $R_2-R_3\approx 1.2$ nm. Along the desorpion isotherm, R_3 starts from a value of $R_3\approx 3.6$ nm at the pore evaporation pressure ($p/p_0\approx 0.58$), meeting almost exactly the corresponding value on the adsorption branch at this pressure. At pressures below pore evaporation, the values of R_3 and α derived from the desorption scan are practically identical with those of the adsorption scan.

The quality of the fit is indicated by the values of the variance χ^2 in Fig. 6(c). It is seen that χ^2 is small in the pressure range up to about $p/p_0\approx 0.5$, but increases strongly above this pressure in a region still well below the lower closure point of the hysteresis loop. The quality of the fit cannot be improved by introducing a Debye-Waller factor, nor by using Eq. (10) instead of Eq. (8), i.e., assuming that a fraction of (smaller) pores may already be filled at lower pressures. In fact, the parameter γ of Eq. (10), when used as a free fit parameter, remains zero up to pressures very close to the capillary condensation region, and then jumps suddenly from zero to one, in agreement with the expected behavior. However, the present model cannot describe the data properly in the pressure region close to the phase transition. Accordingly, the values of R_3 above $p/p_0\approx 0.5$ should be taken with some caution.

IV. DISCUSSION

In situ synchrotron small-angle diffraction along adsorption and desorption scans of an organic liquid (C_5F_{12}) in SBA-15 silica at room temperature delivers high-quality diffraction patterns. Up to seven diffraction peaks from the two-dimensional hexagonal lattice of mesopores are clearly resolved, allowing the development of a detailed structural model for the evacuated silica matrix and for liquid film growth at the pore walls as the vapor pressure is increased. In the following, the results of the evacuated material and the different stages of pore filling are compared with recent studies from literature. In particular, the differences between the present and previous treatments are discussed and the limitations of the employed model for pressures close to the phase transition are commented.

A. Evacuated sample

For the evacuated SBA-15 sample, the present study supports the findings of Impéror-Clerc *et al.*[19] that a model based on ideal cylindrical pores embedded in the bulk silica matrix (two-density-level model) and a Debye-Waller factor (accounting for the nonideality of the periodic pore structure) cannot represent the peak intensity data in a satisfactory way. In agreement with the present results, these authors obtained a good fit of their data by a model involving a corona of uniform density without including a Debye-Waller factor. Figure 5 indeed shows that also the integrated intensities of the (22) and (31) peaks (which were not resolved in earlier studies) are well represented by the model. The value of R_2 obtained in this way is in reasonable agreement with the pore radius as derived from the nitrogen sorption isotherm on the basis of the density functional theory (R_{DFT}) or the conventional BJH analysis (R_{BJH}) (Table I). The values of R_1 and R_2 in Table I yield a total wall thickness $a-2R_2=3.74$ nm and a corona thickness $R_1-R_2=1.2$ nm. From the value of the mi-

croporosity P in combination with R_1 and R_2, one finds that the micropore volume of the corona represents about 22% of the total pore volume of the sample. This value is significantly higher than the value derived from the nitrogen sorption isotherm by the *t*-plot method,[6] which gives a specific micropore volume of 0.062 $cm^3\,g^{-1}$ (about 6% of the total pore volume). This difference may be attributed to the fact that the mean density of the corona is affected not only by microporosity but also by surface corrugations of the pore walls which may not contribute to the micopore volume determined by gas adsorption (see Sec. IV B).

It is of interest to compare the present results with those of sample P123 BC reported by Impéror-Clerc *et al.*,[19] as this sample was prepared in a similar way as in this study (Table I). The values of both R_1 and R_2 of the present sample are somewhat larger (both in absolute terms and relative to the lattice parameter a), but the microporosity P is smaller than for P123 BC. This difference is expected in view of the longer thermal post-treatment of the present specimen. Impéror-Clerc *et al.* found that a model involving a corona of linearly increasing radial density yields similar values of the pore radius and an equally good fit of the data as the model involving a corona of constant density. This is to be expected if $P \approx 0.5$ (i.e., $\alpha = \rho_1/\rho_0 \approx 0.5$) which was indeed the case for the samples studied by these authors. However, extended thermal post-treatment of the SBA-15 leads to samples of lower microporosity of the corona, as in the present study ($P=0.41$). In this case, the model involving a corona of linearly increasing radial density becomes physically less meaningful than the model of a corona of constant mean density, adopted in the present work.

B. Pore filling

The determination of the corona density, expressed by the parameter α, and the film thickness $R_3 - R_2$ as a function of relative pressure of the adsorbed fluid (Fig. 6) represents the main result of the present study. To our knowledge the paper of Albouy and Ayral[13] on the sorption of nitrogen in MCM-41 and the recent work of Hofmann *et al.*[12] on the sorption of krypton in SBA-15 are the only published x-ray studies of this kind. Albouy and Ayral reported a careful first *in situ* study of N_2 sorption at 77.4 K in MCM-41.[13] Unfortunately, only the first-order reflection could be analyzed quantitatively with respect to the integrated intensity, and thus, only a very simple structural model could be employed. Nonetheless, since MCM-41 exhibits much smoother pore walls than SBA-15, the simple two-step model seems to describe the film growth in MCM-41 quite reliably. Hofmann *et al.*[12] measured up to five diffraction peaks from SBA-15, using an *in situ* sorption setup mounted at a rotating-anode generator, but the statistical accuracy of the two weakest diffraction peaks (21) and (30) was rather low due to the more demanding experimental requirements of low-temperature sorption studies. Accordingly, in the work of Hofmann *et al.* the modeling of the pore structure and adsorbate was dictated by the necessity to reduce the number of fit parameters. Based on the fact that liquid krypton nearly matches the electron density of the silica matrix, they adopted two of the models proposed by Impéror-Clerc *et al.* to interpret the krypton adsorption data over the whole range of pore filling. In both models the formation of an adsorbed film at the pore walls was accounted for by allowing the radius r_1 of the cylinders to decrease with increasing vapor pressure. Their model (A) was based on two density levels and assumed ideal cylindrical pores on a nonideal lattice, with a Debye-Waller factor accounting for this nonideality, while model (B) assumed an ideal lattice of cylindrical objects with a region of linearly increasing density in a range $r_1 \pm \delta$. For the evacuated SBA-15 sample, model B gave a mean pore radius $r_1 = 4.2$ nm in agreement with the value of R_2 in Table I and a corona thickness $2\delta = 2.2$ nm, which is about a factor of 2 greater than $R_1 - R_2 = 1.2$ nm. This difference is expected because the present model assumes a corona of uniform density instead of a radially increasing density assumed in model B of Hofmann *et al.* In addition, the limiting values of r_1 at capillary condensation ($r_1 = 3.2$ nm) and at pore evaporation ($r_1 = 3.5$ nm) found by Hofmann *et al.* are also well compatible with the corresponding values in the present work ($R_3 = 3.3$ and 3.6 nm, respectively). It was not possible to test the model used by Hofmann *et al.* with the present data for C_5F_{12}, as this liquid has a significantly smaller electron density than silica ($\beta = 0.717$) and thus no contrast matching with the matrix occurs. However, the present work confirms the conclusion of Impéror-Clerc *et al.* that a simple two-density level model such as model A of Hofmann *et al.* does not provide a satisfactory fit of the data, even for the evacuated SBA-15 specimen. In particular, higher-order diffraction peaks cannot be reproduced by such a simple model. Moreover, in both models used by Hofmann *et al.* only one of the two parameters (radius r_1) has a clear physical meaning while the meaning of the second parameter (viz., the displacement u in model A and the profile half-width δ in model B) changes with the degree of pore filling. Specifically, the parameter δ of model B represents the half-width of the silica corona for the evacuated silica sample, but the half-width of the vapor/liquid interface of the adsorbed film at pore fillings close to the capillary condensation. Hence the interpretation of δ at intermediate pore fillings is not clear.

In the present work, due to the extended data set accessible by the use of synchrotron radiation, it is not necessary to reduce the number of parameters in such a drastic manner. Instead, a model is chosen in which the number of parameters is sufficient to represent the three geometrical phases (silica, liquidlike film, and pore space) and to allow for the existence of a corona of reduced matrix density around the pores. The chosen four-density-level model is perhaps the simplest way to account for this complex situation. With this model the experimental data can be represented rather well for pressures up to the phase transition. However, on the basis of this model it is not possible to distinguish unambiguously between a microporous corona and highly corrugated pore walls. In the case of a truly microporous corona one would expect that the filling of the corona is completed at relative pressures below the region of film growth. Figure 6 shows, however, that the filling of the corona (increase of parameter α) and the growth of a film (decrease of radius R_3) occur simultaneously in a rather wide range of relative pressure. Such a behavior is indeed expected for highly corru-

gated pore walls, due to a concomitant smoothing of the rough surface together with the growth of a liquid film. This scenario is described equally well with the present model and is suggested by the results in Figs. 6(a) and 6(b), since otherwise one would expect first an increase of α until almost saturation at constant R_3, followed by film growth at constant α. Hence the results of Fig. 6 indicate that separate micropore filling occurs at $p/p_0 < 0.05$, while the concomitant change of α and R_3 at $p/p_0 > 0.05$ is caused by the gradual smoothing of a liquid film with average thickness $R_2 - R_3$. This interpretation is consistent with the fact that the micropore volume as derived from the corona porosity is significantly higher than the micropore volume as obtained from nitrogen sorption (see Sec. IV A). On the other hand, these results imply that interpretation of the parameters α and R_3 in terms of micropore filling and film thickness becomes somewhat blurred at $p/p_0 > 0.5$.

The quality of the fit of our data by the chosen model is excellent at relative pressures up to $p/p_0 \approx 0.4-0.5$, but gets successively worse as the film thickness approaches 1 nm [Fig. 6(c)]. This is surprising at first sight, as one expects that a liquidlike film will cause a smoothing of the pore walls and thus the chosen slab model of the film should be a good approximation for relatively thick films. The strong increase of the variance χ^2 at pressures approaching the phase transition indicates that the chosen model is not sufficient to describe the data in this pressure range. Curve fitting diagrams like those in Fig. 5 reveal that the high variance χ^2 in this pressure range is mostly due to the diffraction peaks at higher q values, which are not properly fitted by the model. Qualitatively, this indicates that the chosen model is not able to reproduce some features on a short length scale, such as fluctuations in the thickness of the adsorbed film. Such fluctuations are expected to become significant in the range of metastable films just before capillary condensation. This means, in particular, that the simple model of a liquid film growing with increasing vapor pressure until capillary condensation might be a too simple picture for the adsorption of organic molecules in the narrow mesopores of SBA-15. Alternatively, a nonuniform film thickness may also be a consequence of insufficient equilibration of the adsorbate in the pores. In this context it is remarkable that the pressure range in which the variance χ^2 of the data fit is high coincides with the range in which we find a significant difference in the integrated intensities of the peaks (22) and (31) measured along adsorption and desorption scans (Fig. 3). This observation indicates that (i) the system may not be fully equilibrated in this pressure range and (ii) the peaks at the high-q end of the experimental range are most sensitive to such deviations. Further systematic studies of the pressure region close to capillary condensation are necessary to resolve these questions.

V. CONCLUSION

The pore structure of SBA-15 periodic mesoporous silica and the different stages of pore filling by an organic fluid have been studied by *in situ* small-angle synchrotron diffraction. The integrated intensities of seven diffraction peaks resulting from the two-dimensional hexagonal packing of the cylindrical mesopores can be measured as a function of the pressure of the adsorbed fluid. Over a wide range of relative pressures the data can be described by a structural model which represents an extension of a corona model for pure SBA-15 proposed by Impéror-Clerc *et al.*,[19] by considering adsorption into this corona and the growth of a liquid-like film at the walls of the cylindrical mesopores. The analysis shows that only in the very low-pressure region of the isotherm ($p/p_0 < 0.05$) adsorption leads to an increasing density of the corona, indicating micropore filling. Subsequently, in a relatively wide pressure range adsorption into the corona and the growth of the film thickness occur simultaneously, as to be expected for highly corrugated pore walls. Beyond this regime the film thickness continues to grow with increasing vapor pressure and the film thickness is significantly greater at capillary condensation than at the lower closure point of the hysteresis loop, in agreement with theoretical predictions. However, in the pressure range close to the phase transition of the fluid in the pore the quality of the fit deteriorates as indicated by a strong increase of the variance χ^2. Tentatively, this is attributed to a failure of the simple slab model of the adsorbed film at pressures close to the phase transition.

The diffraction data of the evacuated SBA-15 sample can be represented accurately by the underlying model of a corona of uniform density. The analysis yields a corona porosity of approx. 40% and a thickness of approx. 1 nm. The value of the pore radius (inner radius of the corona) resulting from this model agrees within a few percent with the pore radius derived from the nitrogen adsorption isotherm on the basis of the NLDFT theory. This mutual consistency of these two independent methods of pore-size determination is another important finding of the present work.

ACKNOWLEDGMENTS

The authors thank E.-P. Resewitz and M. Taherkhani (Stranski Laboratory) for providing assistance with the construction and the tests of the *in situ* sorption apparatus, and M. Dommach (DESY/HASYLAB) for technical support at the A2 beamline. The authors are indebted to A. Schreiber (Porotec GmbH, Hofheim, Germany) for a characterization of the SBA-15 sample by nitrogen adsorption and M. Thommes (Quantachrome Instruments, Boynton Beach, FL, USA) for performing the NLDFT analysis of the nitrogen isotherm data. Financial support from the Deutsche Forschungsgemeinschaft through SFB 448, and the Max Planck Society is also gratefully acknowledged.

*Electronic address: Oskar.Paris@mpikg.mpg.de

[1] T. J. Barton, L. M. Bull, W. G. Klemperer, D. A. Loy, B. McEnaney, M. Misono, P. A. Monson, G. Pez, G. W. Scherer, J. C. Vartulli, and O. M. Yaghi, Chem. Mater. **11**, 2633 (1999).
[2] P. Selvam, S. K. Bhatia, and C. G. Sonwane, Ind. Eng. Chem. Res. **40**, 3237 (2001).
[3] S. J. Gregg and K. S. W. Sing, *Adsorption, Surface Area and Porosity* (Academic, New York, 1982).
[4] L. D. Gelb, K. E. Gubbins, R. Radhakrishnan, and M. Sliwinska-Bartkowiak, Rep. Prog. Phys. **62**, 1573 (1999).
[5] A. V. Neimark, P. I. Ravikovitch, and A. Vishnyakov, J. Phys.: Condens. Matter **15**, 347 (2003).
[6] S. Lowell, J. E. Shields, M. A. Thomas, and M. Thommes, *Characterization of Porous Solids and Powders: Surface Area, Pore Size and Density* (Kluwer Academic Publishers, Dordrecht, 2004).
[7] W. H. Lawnik, U. D. Goepel, A. K. Klauk, and G. H. Findenegg, Langmuir **11**, 3075 (1995).
[8] W. Prange, W. Press, M. Tolan, and C. Gutt, Eur. Phys. J. E **15**, 13 (2004).
[9] V. Panella and J. Krim, Phys. Rev. E **49**, 4179 (1994).
[10] A. C. Mitropoulos, J. M. Haynes, R. M. Richardson, and N. K. Kanellopoulos, Phys. Rev. B **52**, 10035 (1995).
[11] G. Dolino, D. Bellet, and C. Faivre, Phys. Rev. B **54**, 17919 (1996).
[12] T. Hofmann, D. Wallacher, P. Huber, R. Birringer, K. Knorr, A. Schreiber, and G. H. Findenegg, Phys. Rev. B **72**, 064122 (2005).
[13] P.-A. Albouy and A. Ayral, Chem. Mater. **14**, 3391 (2002).
[14] E. Hoinkis, Langmuir **12**, 4299 (1996).
[15] J. D. F. Ramsay and S. Kallus, J. Non-Cryst. Solids **285**, 142 (2001).
[16] B. Smarsly, C. Göltner, M. Antonietti, W. Ruland, and E. Hoinkis, J. Phys. Chem. B **105**, 831 (2001).
[17] E. Hoinkis, Part. Part. Syst. Charact. **21**, 80 (2004).
[18] B. Smarsly, M. Thommes, P. I. Ravikovitch, and A. V. Neimark, Adsorption **11**, 653 (2005).
[19] M. Impéror-Clerc, P. Davidson, and A. Davidson, J. Am. Chem. Soc. **122**, 11925 (2000).
[20] A. Schreiber, I. Ketelsen, G. H. Findenegg, and E. Hoinkis, Stud. Surf. Sci. Catal. **30**, 17 (2006).
[21] A. V. Neimark, P. I. Ravikovitch, and A. Vishnyakov, Phys. Rev. E **62**, R1493 (2000).
[22] K. Morishige and M. Ito, J. Chem. Phys. **117**, 8036 (2002).
[23] A. Schreiber, H. Bock, M. Schoen, and G. H. Findenegg, Mol. Phys. **100**, 2097 (2002).
[24] M. Thommes, R. Köhn, and M. Fröba, Appl. Surf. Sci. **196**, 239 (2002).
[25] J. M. Esparza, M. L. Ojeda, A. Campero, A. Domínguez, I. Kornhauser, F. Rojas, A. M. Vidales, R. H. López, and G. Zgrablich, Colloids Surf., A **241**, 35 (2004).
[26] K. J. Edler, P. A. Reynolds, and J. W. White, J. Phys. Chem. B **102**, 3676 (1998).
[27] P. Feng, X. Bu, and D. J. Pine, Langmuir **16**, 5304 (2000).
[28] M. Kruk, M. Jaroniec, C. H. Ko, and R. Ryoo, Chem. Mater. **12**, 1961 (2000).
[29] P. I. Ravikovitch and A. V. Neimark, J. Phys. Chem. B **105**, 6817 (2001).
[30] A. Galarneau, H. Cambon, F. Di Renzo, R. Ryoo, M. Choi, and F. Fajula, New J. Chem. **27**, 73 (2003).
[31] M. Kruk, M. Jaroniec, and A. Sayari, Langmuir **13**, 6267 (1997).
[32] I. G. Shenderovich, G. Buntkowsky, A. Schreiber, E. Gedat, S. Sharif, J. Albrecht, N. S. Golubev, G. H. Findenegg, and H.-H. Limbach, J. Phys. Chem. B **107**, 11924 (2003).
[33] D. Zhao, J. Feng, Q. Huo, N. Melosh, G. H. Fredrickson, B. F. Chmelka, and G. D. Stucky, Science **279**, 548 (1998).
[34] D. Zhao, Q. Huo, J. Feng, B. F. Chmelka, and G. D. Stucky, J. Am. Chem. Soc. **120**, 6024 (1998).
[35] S. Gross and G. H. Findenegg, Ber. Bunsenges. Phys. Chem. **101**, 1726 (1997).
[36] Computer code HP VEE, Hewlett-Packard, Palo Alto, CA, USA, 1995.
[37] G. Elsner, C. Riekel, and H. G. Zachmann, Adv. Polym. Sci. **67**, 1 (1985).
[38] A. P. Hammersley, S. O. Svensson, M. Hanfland, A. N. Fitch, and D. Häusermann, High Press. Res. **14**, 235 (1996).
[39] Computer code PYTHON, Python Software Foundation, Ipswich, MA, USA, 2004.
[40] T. Williams and C. Kelley, Computer code GNUPLOT, http://www.gnuplot.info, 2004.
[41] J. S. Pedersen, Adv. Colloid Interface Sci. **70**, 171 (1997).
[42] O. Glatter and O. Kratky, *Small Angle X-ray Scattering* (Academic Press, London, 1982).
[43] Computer code MATHEMATICA, Wolfram Research, Champaign, IL, USA, 2005.